Chapter 8

What Are the Origins of V-Shaped (Chevron) Dunes in Madagascar? The Case for Their Deposition by a Holocene Megatsunami

D. Abbott[1, 2]

V. Gusiakov[3]

G. Rambolamanana[4]

D. Breger[2, 5]

R. Mazumder[6]

K. Galinskaya[7]

[1]City College of New York, New York, NY, United States

[2]Lamont-Doherty Earth Observatory of Columbia University, Palisades, NY, United States

[3]Tsunami Laboratory, ICMMG SD RAS, Novosibirsk, Russia

[4]University of Antananarivo, Madagascar

[5]Micrographic Arts, Saratoga Springs, NY, United States

[6]Curtin University, Miri, Sarawak, Malaysia

[7]Brooklyn College, New York, NY, United States

Acknowledgments

We thank WAPMERR for funding our 2006 Expedition to Madagascar. We thank Andriamiranto Raveloson and Hoby Razafinodrakoto for their invaluable assistance in the field. We thank W. Bruce Masse, Ann Isley and A.J. van Loon for helpful suggestions that improved the text. We thank the Museum of Natural History in New York City for access to their microprobe facility. We thank the City College of New York for access to their scanning electron microscope facility. We are grateful to the late Jeff Steiner who was responsible for creating this wonderful facility and for sponsoring our initial access. We thank Tom Guilderson and the Center for AMS dating at Lawrence Livermore National Laboratory for their careful analyses of our carbonate-rich sand. We thank Kara Dennis for help with calcium carbonate analyses. We thank Leanne Darson for grain size analyses and for picking fossils for thin sections. We thank the Earth Institute for support of salary costs for Leanne. We thank NSF grant OCE-13-59194 for support of Karina Galinskaya, the AMS ^{14}C dating, and carbonate analyses.

1 Introduction

Chevrons are elongated dunes with a V-shaped pattern in map view. In some exposures, smaller Vs are nested within the larger Vs. The term chevron was first used to describe desert dunes (Maxwell and Haynes, 1989) based on their similarity to the nested chevrons used on military uniforms or in heraldry. Chevrons later were identified in coastal regions and proposed to represent megastorm deposits (Hearty et al., 1998; Kindler and Strasser, 2000). Subsequently, other workers suggested that some coastal chevron dunes were tsunami deposits (Bryant and Nott, 2001; Scheffers and Kelletat, 2003; Scheffers et al., 2008).

The proposal that some coastal chevron dune complexes represent tsunami deposits is based on three sets of observations (Scheffers and Kelletat, 2003). The first is that the long axes of many coastal chevron complexes are not oriented parallel to the direction of the prevailing wind. The second is that some chevron complexes extend several kilometers (km) inland and rise to over 100 meters (m) above sea level. Some of these chevron complexes are located on shorelines that lack beaches. In these particular cases, it is difficult to understand how either megastorms or wind could have formed the chevrons. Megastorms cannot move subaerial rock and sediment over km-scale distances with elevation gains of hundreds of meters (Cox et al., 2012; Erdmann et al., 2015). Wind cannot move sediment inland if there are no subaerial, poorly consolidated sediments on the coast.

In this chapter, we describe three chevron complexes, V-shaped, elongated dune complexes on the southern coast of Madagascar. Their origin is disputed because individual dunes are elongated along an azimuth that is close to the

direction of the prevailing winds (Abbott et al., 2008; Pinter and Ishman, 2008), although their low angle of deposition generally is inconsistent with aeolian dunes. However, other characteristics preclude their derivation from modern beach deposits, although we do not discount later aeolian reworking of some chevron deposits. In particular, the Madagascar chevrons contain significant proportions of early Holocene carbonate tests resembling shells of marine foraminifera, including some that are partially dolomitized, and some that are infilled with mud. These observations suggest that marine carbonate tests in the chevrons were eroded from the continental shelf, and not from modern beaches. Furthermore, despite having lateral extents of tens of km, characteristics of the chevrons (degree of sediment sorting, carbonate content, and marine microfossil concentrations) do not change significantly along strike, as might be expected for aeolian deposits.

2 Background

We previously hypothesized that the Madagascar chevrons were generated by a megatsunami (Gusiakov et al., 2010), and that either a submarine impact in the vicinity of the Burckle Crater candidate (Abbott et al., 2007) or a caldera collapse of Reunion Island (Oehler et al., 2004) could have produced the postulated megatsunami wave. However, despite our previous assertions (Abbott et al., 2008; Gusiakov et al., 2010), no unequivocal impact component has been identified within the Madagascar chevron sands, and the source of a putative megatsunami wave is presently unknown.

The megatsunami origin of Madagascar chevrons is disputed by others, who favor an aeolian origin (Pinter and Ishman, 2008; Bourgeois and Weiss, 2009). In this chapter, we present further information suggesting that the three dune complexes in Madagascar had a megatsunami origin.

On the southern coast of Madagascar, there are marine fossil-bearing chevron dunes that extend over 40 km along-strike, rising to over 175 m above sea level (Figs. 8.1 and 8.2). During a three-week field reconnaissance in 2006, we examined the three most obvious chevrons having the greatest sand thicknesses: Faux Cap, Fenambosy, and Ampalaza. Our group collected sediment samples and marine shells from the surface of the three chevron complexes, in the subsoil, and nearby, along the southern coast (Fig. 8.1; Table 8.1). As we will show, certain characteristics of the chevrons strongly suggest a megatsunami origin.

elsevier_978-0-12-803386-9_B978-0-12-803386-9_00008-3

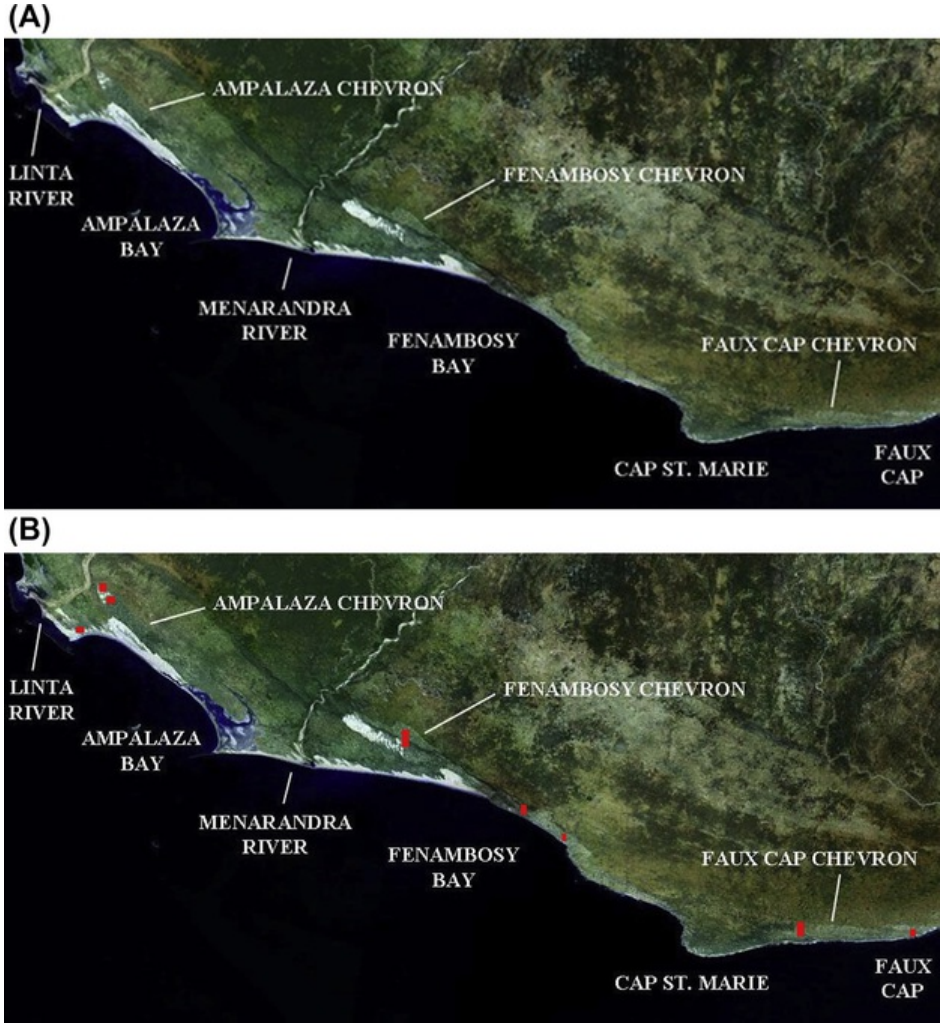

Figure 8.1 Satellite image showing the three Madagascar chevron dune complexes. Due north is up. This image was taken during a time of comparatively high rainfall, thereby maximizing the visual contrast between the chevrons and the surrounding terrain. The reworked parts of the chevrons are white and the vegetated portions are a uniform green that stands out against the brown to greenish-gray color of the surrounding bedrock. (A) Annotated image of chevrons and surroundings. (B) Same image as (A) with sampling sites in red. Both images from 2007 Europa Technologies, 2007 Digital Globe, and 2007 TerraMetrics.

Figure 8.2 Photo (Image © Dallas Abbott) looking northwest showing the fault scarp separating the elevated plateau portion of the Fenambosy Chevron from the lower coastal plain. This photo clearly shows the scarp cliff in two places. The near cliff encompasses chevron deposits that are continuous on the coastal plain and discontinuous along 9 km of the uplifted wall of the fault scarp (cf., the middle red rectangle on Fenambosy Chevron in Fig. 8.1B). These were sampled on one traverse. The far cliff has ubiquitous chevron deposits extending from the coastal plain to the top of the elevated plateau. They cover a 21 km-long section of the fault. The far cliff includes the westernmost red rectangle (sampling sites on the N–S traverse) of the Fenambosy Chevron shown in Fig. 8.1B.

Table 8.1 Locations, Names, and Elevations of Sampling Sites

Location	Latitude	Longitude	Site Name	Elevation, m
Ambondro (not on chevron)	−25.23500	45.79700	S2	204
Fenambosy (not on chevron—on subsoil)	−25.35588	44.86937	S4	79
Fenambosy chevron	−25.36143	44.86712	S5	66
Fenambosy chevron	−25.24112	44.69767	S9	153
Fenambosy chevron	−25.25203	44.69060	S12	186
Fenambosy chevron	−25.26695	44.68449	S13	53
Cap St. Marie (not on chevron)	−25.55711	45.15937	S14	140
Cap St. Marie (not on chevron)	−25.58095	45.16374	S17	194
Ampalaza chevron	−24.98868	44.16132	S19	63
Ampalaza chevron	−25.00429	44.16482	S20	88
Ampalaza chevron	−25.05840	44.12059	S22	6
Ampalaza chevron	−25.00907	44.19189	S25	64

Ampalaza chevron	−25.01003	44.19458	S26	68
Ampalaza chevron (65 cm depth)	−25.01337	44.19415	S27	53
Ampalaza chevron (15 cm depth)	−25.01325	44.19415	S28	55
Ampalaza chevron	−25.01299	44.19082	S30	66
Menarandra River	−25.05565	44.67977	S32A	66
Faux Cap chevron field	−25.554567	45.51968	S32B	10
Faux Cap chevron field	−25.55795	45.51803	S33	17
Faux Cap chevron field	−25.57435	45.29113	S35	61
Faux Cap chevron field	−25.56093	45.28285	S36	150
Faux Cap chevron field	−25.54261	45.27870	S37	205

The Fenambosy Chevron is the most spectacular of the three we sampled. It extends at least 28 km along-strike and has a maximum width of 6 km. It encompasses a steep fault scarp approximately 175 m high (Fig. 8.2). On the elevated portion of the chevron that lies landward of the fault scarp, the edge of the chevron is 6–12 km from the ocean.

3 Sample Selection and Processing

Given that this study provided for initial and rapid reconnaissance of the area, traverse locations largely were constrained to those that were accessible by road. Additionally, the two traverses on the Fenambosy Chevron were located so that people who conducted sampling could safely negotiate the fault scarp cliff on foot. Because local roads are impassable during the wet season, we also timed our trip to coincide with the dry season.

As the weather was dry during our trip, we could not discern sedimentary structures on exposed dune interiors. In most cases, we used a trowel to dig into the surface so that samples represent a mixture of sediment derived from the surface down to several centimeters (cm). At one site on the Ampalaza chevron (S27), we used a shovel to sample at a depth of half a meter to provide for a comparison to near-surface samples.

In the lab, samples were wet-sieved first to remove dust and fine organic carbon. Wastewater from wet sieving was sterilized using bleach to kill potentially dangerous microorganisms. Samples were then dry-sieved using sieves with mesh sizes of 38, 63, 125, 250, and 500 micrometers (μm). If there were significant numbers of particles >500 μm, we used larger sieves to characterize the size distribution of those particles further. Sorting and other sedimentologic parameters were calculated using a statistical package (Blott and Pye, 2001). Due to our relatively small sample sizes, we could not extend our size analyses to grains <38 μm in diameter, therefore our estimates of the degree of sorting are maximum values, as including the silt and clay fractions in our analyses would reduce the estimated degree of sorting.

Our samples of the Madagascar chevrons were taken as far as possible from local farmers' fields. Many samples are, however, only km distant from active agricultural sites. We interviewed the farmers and they indicated that they were not importing marine carbonate into their fields, nor were they eating shellfish. Larger seashells (3–6 cm wide) found on the surface of the dunes in all chevron complexes have modern ^{14}C ages, suggesting that they were collected and brought inland as souvenirs, or that they are residues from subsistence practices several generations in the past. We are skeptical that their ages accurately date the chevron deposits themselves. Consequently, we use the ^{14}C ages of marine microfossils in the deposits to provide a maximum age for chevron deposition, as discussed later in the chapter.

For carbonate analyses, half a gram of unsieved sample was ground and homogenized with a mortar and pestle. Carbonate was assessed in replicate samples using a ~~carbon~~ CO_2 coulometer.

We used a Zeiss Supra 50 scanning electron microscope (SEM) fitted with an EDAX energy-dispersive X-ray microanalyzer (EDS) located at City College in New York City to evaluate individual sediment grains. We looked at both mounted marine microfossils and sediment lithogenic clasts, as well as clasts and microfossils in thin sections.

The high carbonate content of the chevron sands meant that even with relatively small sample sizes (half liter bags), we had enough material for ^{14}C AMS dating. We used the 125–250 μm size fraction of the chevron sand, which contains well-preserved marine microfossil tests and quartz grains. The maximum grain size below which sand grains are transported by continuous suspension in air is 3.5 ϕ or 88 μm (Visher, 1969; Skoček and Saadallah, 1972). Therefore, our dated sands are unlikely to have been transported by the wind except through saltation or grain creep, both of which would destroy the carbonate tests after transport over a few km (Sharp, 1966). All samples were wet-sieved and appeared very clean. Nevertheless, we carefully examined each sample under a microscope and picked out any material that might bias our dating results. We found a few minor pieces of flat carbonate that could either be fragments of marine bivalves or of land snails. These were removed from our samples, as were any pieces of possible terrestrial organic matter. The final samples sent out for dating consisted of a mixture of clean quartz sand and clean marine microfossil tests.

4 Sedimentary Characteristics of Chevron Sands

We compared the fossil content (marine fossils per gram in the 250–500 μm size range) and grain size distribution of surrounding areas to that of the chevrons (Tables 8.2 and 8.3). Land snails are not abundant and constitute <1% of the fossils per gram. Land snails and questionable marine fossils are excluded from the count. All four of the samples from off chevron contain 10% $CaCO_3$ or less and all but one (S14) contain no fossils. The samples from the chevrons all contain fossils and carbonate, typically between 40% and 60% $CaCO_3$ and between 21 and 5750 marine fossils per gram. The three samples with counts of 993–5750 fossils per gram are all from sites within 2 km of the ocean. In each sample, we must sort through tens to hundreds of grains to find a single fossil. For the sample with the most abundant fossils (5750 per gram at S22), we calculate that there are 12 mineral grains per fossil (De Villiers, 2005). For the sample with the next highest abundance of fossils (2236 per gram at S33), we calculate that there are 30 mineral grains per fossil. Therefore, the grain size distribution of these samples is primarily determined by the size distribution of the mineral grains and not by the size distribution of the fossils. Interestingly the three most fossil-rich samples are all moderately well sorted, not well sorted, as would be expected if the bulk sediment were primarily transported by the wind.

Table 8.2 Sedimentologic Parameters of Coarse Silts and Sands From Madagascar[1]

Samples from Fenambosy Chevron ~~S5, S9, S12, S13 (FC)shaded gray~~, from Ampalaza Chevron (AC)S19, S20, S22, S25, S26, S27, S28, S30~~shaded brown,~~ and from Faux Cap Chevron (FCC) S32B, S33, S35, S36, S37~~shaded blue~~.Sites on Fenambosy Chevron: S5, S9, S12, S13. Sites on Ampalaza chevron: S19, S20, S22, S25, S26, S27, S28, S30. Sites on Faux Cap chevron: S32B, S33, S35, S36, S37.

Site#	Mean, ϕ	Sorting, ϕ	Skewedness, ϕ	Kurtosis, ϕ	Sorting
S2 (off)	0.93	0.64	1.64	6.83	MWS
S4 (off)	2.10	1.02	−0.60	4.26	PS
S5 (FC)	1.72	0.57	0.12	~~(FC)~~7.99	MWS
S9 (FC)	1.81	1.07	−0.04	1.80	PS
S12 (FC)	2.45	0.79	−2.60	14.50	MS
S13 (FC)	1.89	0.88	−0.42	3.08	MS
S14 (off)	1.26	0.77	0.29	4.57	MS
S17 (off)	0.89	0.66	0.55	4.83	MWS
S19 (AC)	2.65	0.48	0.41	3.72	WS
S20 (AC)	2.35	0.60	−0.04	3.05	MWS
S22 (AC)	2.91	0.53	−0.01	2.35	MWS
S25 (AC)	2.25	0.68	−0.42	3.99	MWS
S26 (AC)	1.81	0.86	−0.28	2.05	MS
S27 (AC)	2.16	0.80	−0.41	3.07	MS
S28 (AC)	1.79	0.78	0.12	2.90	MS
S30 (AC)	1.91	0.74	−0.72	4.06	MS
S32A (off)	2.34	0.73	−1.11	5.51	MS
S32B (FCC)	2.25	0.66	−0.70	4.19	MWS
S33 (FCC)	2.18	0.74	−1.62	8.05	MS
S35 (FCC)	1.33	0.66	0.59	5.22	MWS
S36 (FCC)	1.32	0.87	0.46	3.85	MS
S37 (FCC)	1.17	1.13	0.79	2.97	PS

[1] These are the results of calculations from the data in Appendix 8.1 using the logarithmic method of moments (Krumbein and Pettijohn, 1938; Blott and Pye, 2001). Degree of sorting ranges from poorly sorted (PS: sorting is 1.0–2.0 ϕ), to moderately sorted (MS: sorting is 0.7–1.0 ϕ), to moderately well sorted (MWS: sorting is 0.5–0.7 ϕ), to well sorted (WS: sorting is 0.35–0.5 ϕ).

Table 8.3 Bulk Carbonate Content Versus Marine Fossil Content >250 μm Size Fraction

Samples from Fenambosy Chevron S5, S9, S12, S13~~shaded gray~~, from Ampalaza Chevron ~~shaded brown~~S19, S20, S22, S25, S26, S27, S28, S30, and from Faux Cap Chevron S32B, S33, S35, S36, S37~~shaded blue~~.

Site# (Off Chevron Locations Noted)	Replicate 1, % $CaCO_3$	Replicate 2, % $CaCO_3$	Average % $CaCO_3$, Rounded to Nearest %	Fossils/Gram Sediment
S2 (off)	0.0	0.0	0	0
S4 (off)	10.0	9.9	10	0
S5	38.6	38.9	39	46
S9	49.2	48.7	49	65
S12	52.5	54.0	53	179
S13	58.3	57.8	58	215
S14 (off)	2.8	3.5	3	0
S17 (off)	8.5	8.8	9	10
S19	40.8	40.8	41	95
S20	48.9	48.3	49	100
S22	53.8	54.2	54	5750
S25	39.4	39.0	39	94
S26	44.6	45.1	45	205
S27	42.5	42.4	42	140
S28	36.0	36.1	36	75
S30	35.1	36.5	36	442
S32A (off)	0.0	0.0	0	0
S32B	40.4	41.2	41	993
S33	52.0	53.4	53	2237
S35	22.6	23.4	23	38
S36	40.0	37.3	39	56
S37	7.4	7.2	7	21

We attribute many of the differences in fossil count to the difficulty of accurately counting fossils whose surfaces have been ablated by later aeolian activity. This hypothesis is consistent with two observations. The first is that the carbonate contents of the fossil-bearing samples vary much less than the fossil counts (Table 8.3). The second is the common occurrence of marine microfossils that are easily identifiable only on one side. At many sites, we observed marine microfossils with significant differences in preservation between their top and bottom surfaces. This pattern may occur because the fossils are too big to be moved by the wind. As a result, saltating sand grains would tend to preferentially erode upper, exposed surfaces. Lower surfaces facing downward would better preserve the distinctive surface morphology of marine benthic foraminifera.

Because the two mineral forms of calcium carbonate, calcite and aragonite, both have cleavage, individual grains are broken into smaller and smaller pieces as they are transported by saltation. In contrast, quartz has no cleavage and

individual grains become more rounded as they are transported by saltation. In an aeolian depositional environment, attrition (collision between grains) is significant and very effective in imparting roundness because the viscosity of air is much lower than that of water (Allen, 1985). As a result, mature aeolian sands and silts consist of nearly pure, rounded quartz grains with minor proportions of heavy minerals and calcium carbonate. If transported by saltation induced by the wind, initially angular quartz and other mineral grains become well-rounded and well-sorted over a relatively short transport distance, about 10–12 km (Sharp, 1966).

In our samples, individual marine carbonate microfossils had ablated surfaces but did not appear broken (Fig. 8.3). Individual sediment clasts that lack cleavage, such as quartz and garnet, were typically angular and irregular, rather than spherical.

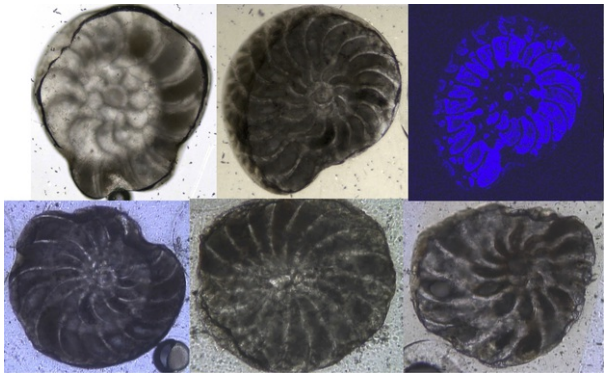

Figure 8.3 Transmitted light images and Mg element map (top right) of marine microfossils in thin section from Madagascar chevrons. All microfossils were picked from the 250–500 μm size fraction. Top: Marine microfossils from northwest distal end of Ampalaza Chevron. Bottom: Marine microfossils from Fenambosy Chevron.

5 Characteristics of Individual Chevrons

5.1 Fenambosy Chevron

The sand dunes making up the Fenambosy Chevron have two distinct morphologies depending on whether they are vegetated or not (Fig. 8.4: top). In unvegetated areas with sand at the surface (appearing white in Fig. 8.4: top), chevrons are being reworked by the wind, and the dunes are elongated perpendicular to the wind direction. In the areas with the maximum erosion from deflation, the slip faces of the dunes have angles up to 30 degrees and the underlying substrate is exposed.

elsevier_978-0-12-803386-9_B978-0-12-803386-9_00008-3

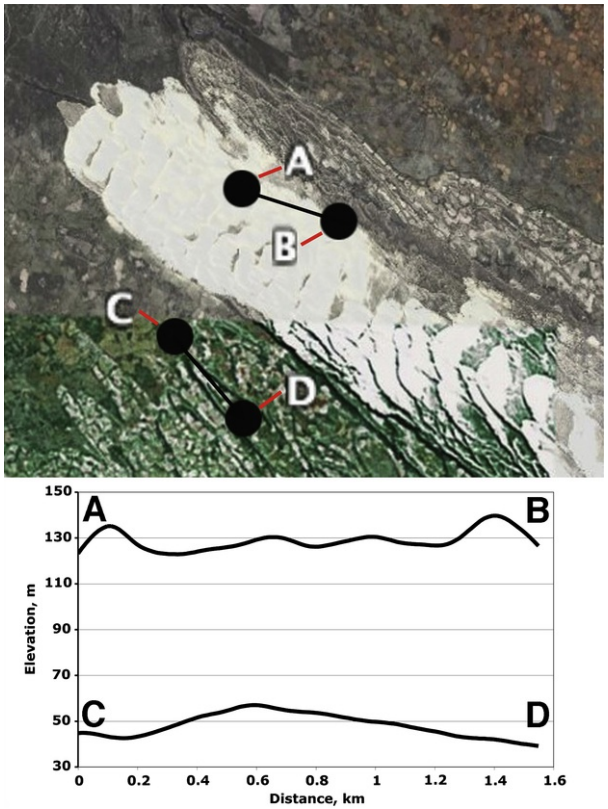

Figure 8.4 Top: Satellite image of far end of Fenambosy Chevron from Google Earth (2007) Europa Technologies (2007), Digital Globe (2007) and TerraMetrics (2007). This image was taken during a time of high rainfall. *Red lines* connect letters to *black circles* at ends of cross-sections. The fault scarp cliff runs NW to SE in the gray area that appears near the base of the letter A. Based on the relative whiteness of the image, the sand layer north of the fault appears thinner than the sand layer south of the fault. (In the field, both areas were covered with sand whose total thickness was difficult to determine.) Bottom: Cross-sections—A–B is from an area of active ablation of the dune surfaces; C–D is from a vegetated area that is not being farmed.

Conversely, chevrons are covered by vegetation in areas that appear light green in satellite photographs (Fig. 8.4: top). In some places, these chevrons are being farmed, producing a patchy appearance derived from the boundaries of farmers' fields. In other greenish areas, the chevrons are covered by undisturbed vegetation and comprise V-shaped structures of varying size and extent. The regions with V-shaped structures have lower relief and smaller maximum surface slopes (about 10 degrees) than the (white) areas of active erosion. Two cross-sections, the first along the long axis of a white area, and the second along the long axis of a green, nonfarmland area, show the contrast in wavelength and surface slope of the dunes (Fig. 8.4: bottom).

The Fenambosy Chevron has a minimum along-strike length of 28 km (Fig. 8.5). If the chevron was exclusively of aeolian origin, we would expect that the quartz grains in the western half of the chevron would be more rounded than those in the eastern half (Sharp, 1966). The western half of the chevron would contain only finely pulverized carbonate grains and would not contain whole, recognizable marine microfossils. Instead we find large numbers of marine microfossils per gram in samples from a distance of >12 km along the strike of the chevron (Table 8.3). The sorting and marine fossil content of the sands in the Fenambosy Chevron vary locally with no significant along-strike trends. This pattern could occur with subaqueous transport but is inconsistent with aeolian transport of the bulk of the material in the chevrons.

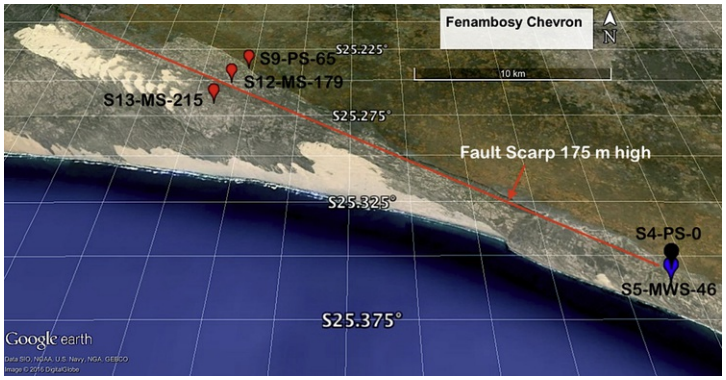

Figure 8.5 Google Earth image of Fenambosy Chevron. Image © 2016 DigitalGlobe. Image © 2016 CNES/Astrium. Colored symbols: Sampling locations color-coded by percentage of $CaCO_3$ in the substrate. Black: 0–20%, Blue: 20–40%, Red: 40–60%. Black lettering: Site#–degree of sorting-number of marine fossils per gram. The degree of sorting is *PS*, poorly sorted; *MS*, moderately sorted. *Black line*-trace of 175-m high fault scarp. Note on right side the two closely spaced sites, S4 and S5. At S4, the substrate to the chevron was exposed. It contains neither $CaCO_3$ nor fossils. Site S5, immediately adjacent, contains 46 fossils per gram of sediment and a significant amount of $CaCO_3$.

In contrast to the well-sorted character of mature aeolian deposits, none of the samples from the Fenambosy Chevron are well sorted (Tables 8.1, 8.2, and 8.3; Fig. 8.6). The black curve with black dots represents the grain size distribution from a Gaussian (normal) curve with the standard deviation of typical well-sorted aeolian sand. The Gaussian curve was calculated using the excel function NORMDIST with the mean set to the mean grain size of each sample in ϕ units and the standard deviation set to 0.425 ϕ: a typical value for well-sorted sediment (Blott and Pye, 2001). The red curves show the grain size distributions derived from sieving bulk samples at 1 ϕ intervals. Most samples contain nearly 100% of material coarser than 38 μm, and grain size distribution results for those samples were not impacted significantly by ignoring the finer than 38 μm component. Only three samples, all located close to the fault scarp, contain large amounts of fine material. As discussed earlier, results for these samples record the maximum degree of sorting since finer-grained materials were discounted.

elsevier_978-0-12-803386-9_B978-0-12-803386-9_00008-3

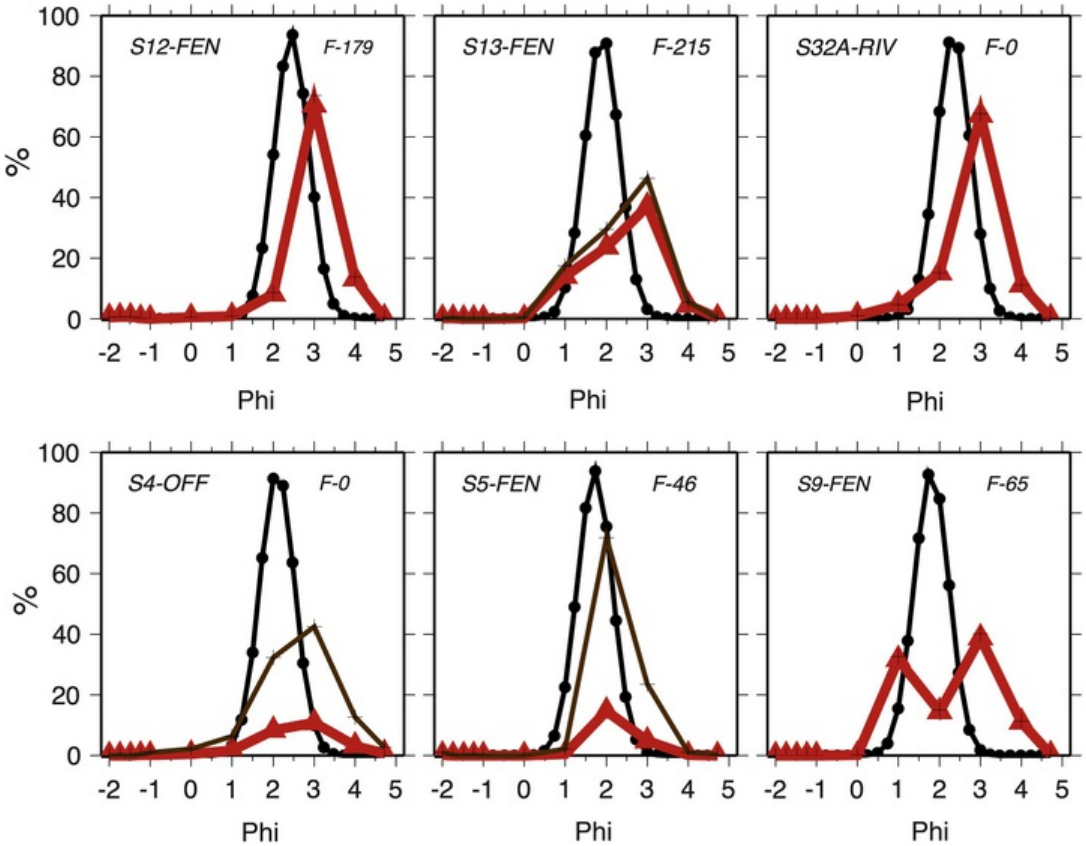

Figure 8.6 Grain size distribution of samples from Fenambosy Chevron compared to samples from the Menarandra River (upper right; S32A-RIV) and to samples from off chevron (lower left; S4-OFF). *Black line* with *black dots*: Theoretical model of the grain size distribution of a well-sorted sand—a normal distribution with the same mean grain size as the sample. *Red line* with *triangles*: Grain size distribution uncorrected for unsieved fine material <38 μm in size. *Brown line* with *crosses*: Grain size distribution corrected to 100%, accounting for material washed through the 38 μm sieve, so not applicable to all samples. *F*, fossils per gram.

We also show a reference sample taken from the Menarandra River (Figs. 8.1 and 8.6), recovered while traveling from the Fenambosy to the Ampalaza Chevron. The sample from the Menarandra River was taken upstream of the western end of the Fenambosy Chevron (Fig. 8.7), thus its primary sediment source is weathered material from the basement and its primary mode of transport is aquatic. The grain size distributions of two of the sediment samples from the Fenambosy Chevron, S12 and S5 (the latter corrected to 100%), closely resemble the grain size distribution of fluvial sediments from the Menarandra River (Fig. 8.6). The sorting of the remaining sediments from the Fenambosy Chevron (S13 = moderately sorted and S9 = poorly sorted) more closely resembles the moderately well-sorted river sediments than well-sorted aeolian sediments.

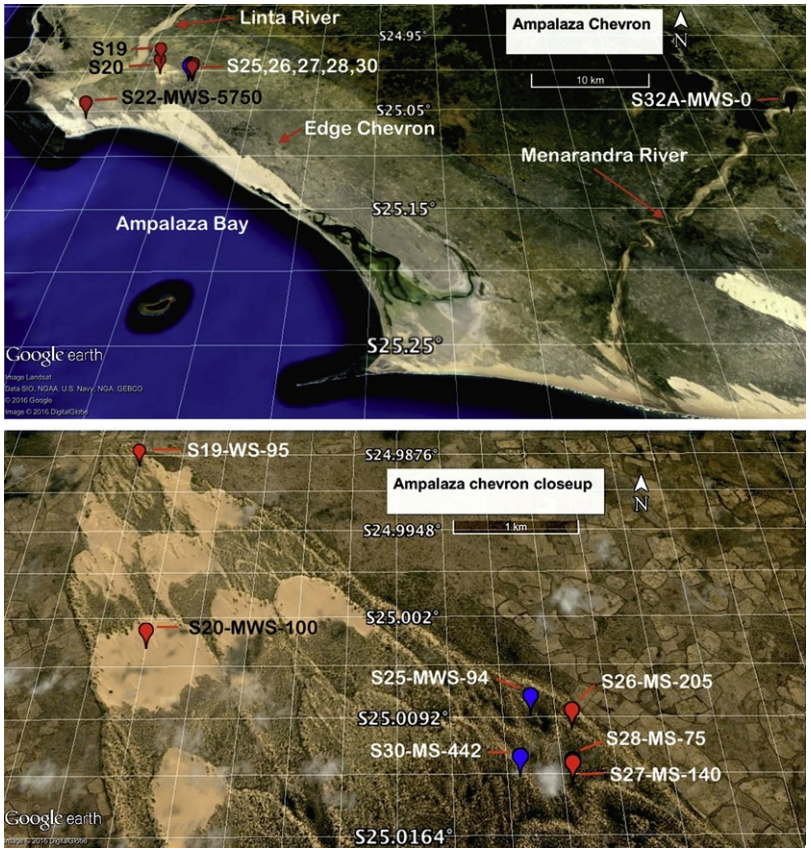

Figure 8.7 Satellite images of the Ampalaza Chevron from Google Earth. Images © 2016 DigitalGlobe. Image © 2016 CNES/Astrium. Colored symbols: Sampling locations color-coded by percentage of $CaCO_3$ in the substrate. Black: 0–20%, Blue: 20–40%, Red: 40–60%. Black and white lettering: Site#-degree of sorting-number of marine fossils per gram. The degree of sorting is *MS*, moderately sorted; *MWS*, moderately well sorted. Top: View of entire chevron. Bottom: Enlargement of detailed sampling area on upper left of top image. The grayish-brown colored, vegetated portion of the chevron is covered with V-shaped sand waves with structure at different scales. White lettering: degree of sorting-number of marine fossils per gram. The sands are *MS*, moderately sorted; *MWS*, moderately well sorted; *WS*, well sorted.

6 Ampalaza Chevron

The Ampalaza Chevron is the longest of those investigated in this study (Fig. 8.7). It extends at least 45 km along-strike and varies from approximately 4 to 6 km wide. Our observations of white, unvegetated areas recorded in satellite photographs demonstrate they are experiencing enough wind erosion to expose the substrate locally, and to transport some sand. The only well-sorted sample on the Ampalaza Chevron is from its northwestern end in one of the unvegetated, white areas (Sample S19; Figs. 8.7 and 8.8). Although the sample is well sorted, it contains about 95 fossils per gram of sample. It was collected at 68 m elevation, well above the 3–5 m maximum rise of Holocene sea level (Camoin et al., 2004; Woodroffe and Horton, 2005) and of the Linta River to the north (Fig. 8.1).

elsevier_978-0-12-803386-9_B978-0-12-803386-9_00008-3

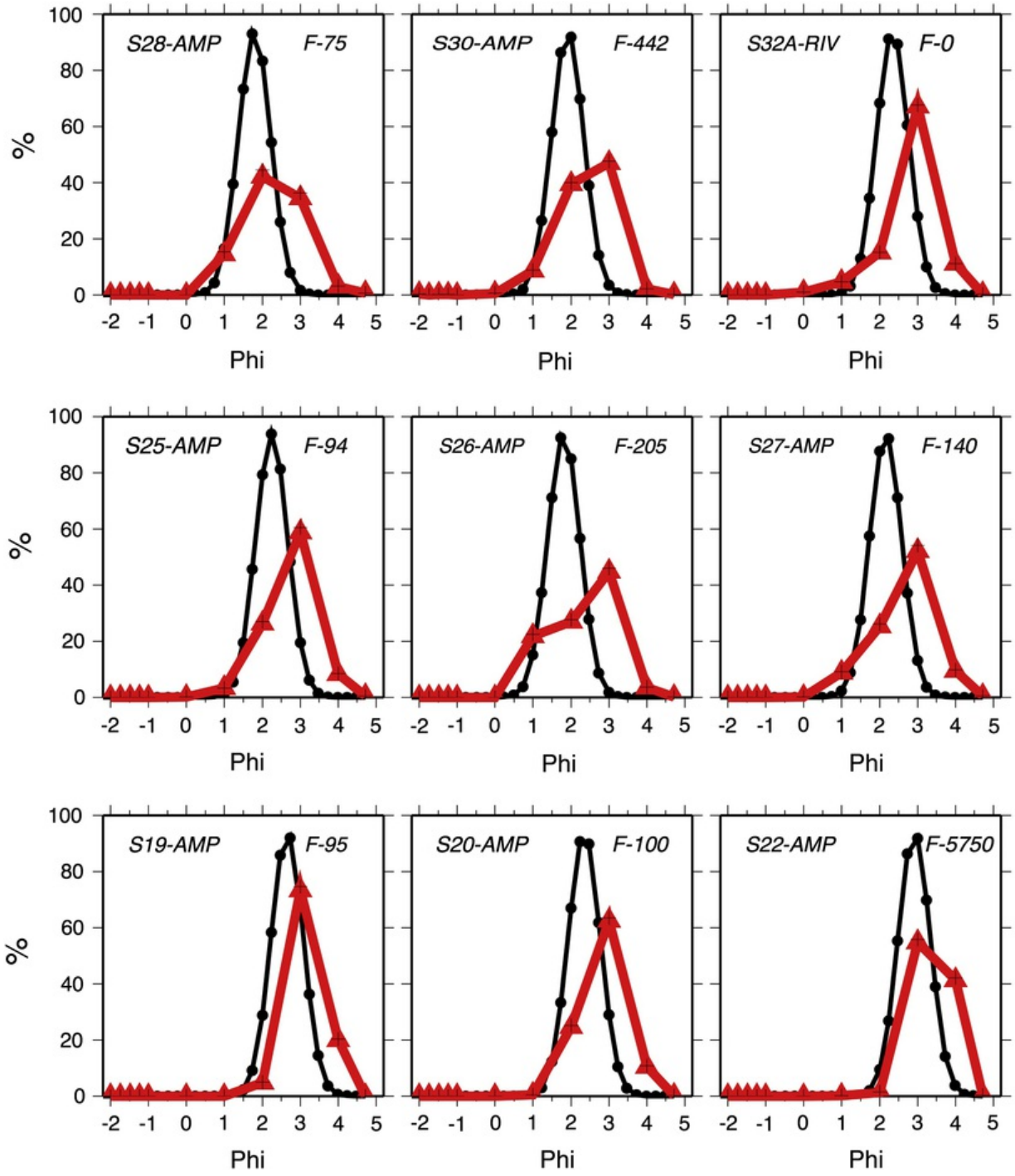

Figure 8.8 Grain size distribution of samples from the Ampalaza Chevron compared to samples from the Menarandra River (S32A, upper right). *Black line* with *black dots*: Theoretical model of the grain size distribution of a well-sorted sand-a normal (Gaussian) distribution with the same mean grain size as the sample. *Red line* with *triangles*: Grain size distribution uncorrected for unsieved fine material below 38 μm in size. *F*, fossils per gram.

The areas of the Ampalaza Chevron covered by vegetation appear dark gray and gray in Fig. 8.7. There are numerous, low-relief, V-shaped hills within the vegetated areas of the chevron. The Vs point toward the uphill, distal end of the chevron. As within the Fenambosy Chevron, aeolian reworking is destroying the V-shaped hills (Fig. 8.7).

The marine fossil content of the Ampalaza Chevron shows no significant trends along-strike. Individual samples are highly variable, with between 75 and 445 fossils per gram in a small area (Fig. 8.7: bottom).

None of the grain size distributions of the sediments in the Ampalaza Chevron match the theoretical distribution of a well-sorted aeolian sediment (Fig. 8.8, *black curves* with *dots*), even the sample characterized as well sorted (S19). All ~~the~~ distributions show a substantial proportion of very fine-grained sand-sized sediment (63–125 μm, $\phi = 3.0–4.0$). The proportion of very fine-grained sand-sized material typically increases with marine fossil content. Coarse-grained sand-sized material (500–1000 μm, $\phi = 0.0–1.0$) occurs in the sample of river sediment, and in all but one of the samples taken from vegetated areas (S26, S27, S28, S30). Two samples are from the same location, S27 from 65 cm depth and S28 from 15 cm depth. These samples demonstrate that the grain size distribution of the dune sand may vary with depth. Overall, the grain size distributions in the Ampalaza Chevron show a closer match to the sediment from the Menarandra River (Figs. 8.7 and 8.8) than to the theoretical grain size distribution of aeolian sediment. The sample from the Menarandra River is from a location well upstream of the Fenambosy Chevron, so it probably represents primary material eroded from the basement. This material is most likely the source of mineral grains in modern, nearby beaches and in early Holocene beach sand incorporated into the Ampalaza Chevron.

The fossils within the chevron have ablated surfaces but are still recognizable as marine microfossils, most likely benthic foraminifers. The interiors of the fossils from the chevron sands are often filled, sometimes with Mg-rich material (Fig. 8.9). Outside the chevron, near the ocean, there are sandy, modern beach deposits. The beach sands have a higher fossil content, with thousands of fossils per gram of sediment. S22 is an example. S22 is somewhat landward of the beach but is within reach of coastal flooding from large storms. The marine microfossils in the beach deposits are hollow, lacking an interior filling. Their surfaces are fresh and are not ablated, unlike the marine microfossils within the chevron sands. These differences suggest that the fossils within the Ampalaza Chevron, although geologically young, are not aeolian deposits derived from modern beaches. Instead they represent marine microfossils that were buried, filled, and altered in situ in the marine environment, perhaps on the continental shelf or below the water table on beaches, and were later excavated and deposited within the chevrons.

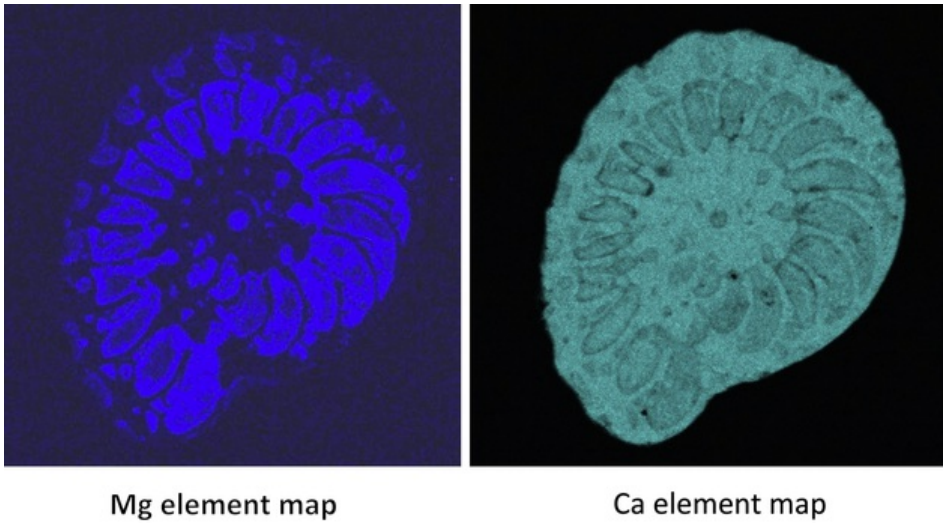

Figure 8.9 Element maps of a thin section of a marine microfossil from the distal end of the Ampalaza Chevron. Unaltered calcium carbonate tests of marine microorganisms typically contain too little Mg for the Mg to show up on an element map. (An element needs to be present above the 1% level to be visible in an element map.) The chambers in the microfossil were probably filled with Mg-rich mud after the organism died. Note that some parts of the test also appear Mg-rich, consistent with partial dolomitization of the test.

An EDS element map of a thin section of a marine microfossil from the distal end of the Ampalaza Chevron (sample labeled MWS-100 in Fig. 8.8) shows the outline of a carbonate-rich microfossil test and its interior, the latter filled with Mg-rich material (Fig. 8.9). Note that the shape of the test appears normal; that is, the test does not appear to be significantly ablated or broken.

The Faux Cap Chevron field differs from the Ampalaza and Fenambosy Chevrons, and is more like the chevrons in the rest of Madagascar. Sand deposits are thinner than in the Ampalaza and Fenambosy Chevrons. This may reflect absence of a significant fluvial sand source, and the more nearly perpendicular orientation of the coastline relative to the direction of sediment transport during a putative megatsunami event. Except for very close to the coast, most of the sand

contains very few marine microfossils. Due to extensive farming, the Faux Cap Chevrons preserve little of the internal V-shaped structures observed in the Fenambosy and Ampalaza Chevrons (Fig. 8.10). V-shapes are faintly visible in the outlines of the Faux Cap Chevrons.

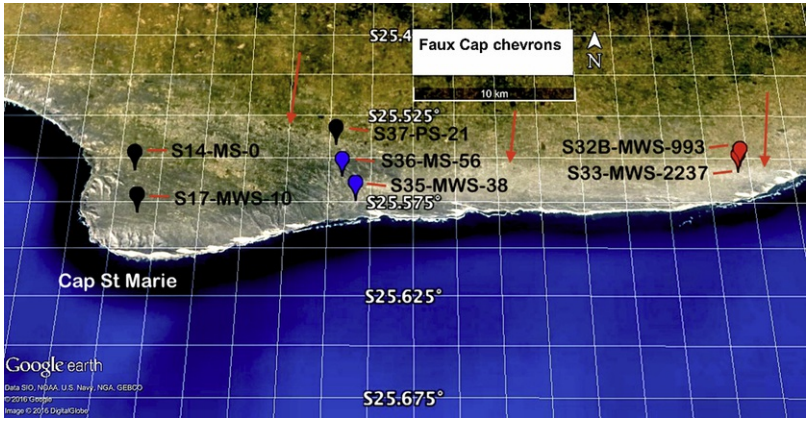

Figure 8.10 Images of the Faux Cap Chevron from Google Earth. Image © 2016 DigitalGlobe. Image © 2016 CNES/Astrium. Regional view. Colored symbols: Sampling locations color-coded by percentage of $CaCO_3$ in the substrate. Black: 0–20%, Blue: 20–40%, Red: 40–60%. Black lettering: Site#-degree of sorting-number of marine fossils per gram. The degree of sorting is *PS*, poorly sorted; *MS*, moderately sorted; *MWS*, moderately well sorted.

The sands lacking marine microfossils contain <10% calcium carbonate. These include sand without $CaCO_3$ from the Menarandra River (Fig. 8.1), sampled in a location landward of the chevrons (Fig. 8.7: top). This observation implies that the calcium carbonate in the chevrons is not derived from nearby basement outcrops. Most likely, all the carbonate in the chevrons was originally eroded from local beach and shallow water sediments. The bulk of the fossils would have come from buried fossils within the beach and shelf sand, and would be expected to have some sediment infilling.

The grain size distributions of the sediments from the Faux Cap chevrons (Fig. 8.11) more closely resemble the fluvial material than well-sorted aeolian sand. Thus, the grain size distributions of the chevron sediment are consistent with their transport by water. The samples from the Faux Cap region (Figs. 8.10 and 8.11) also include two examples of sediments from locations close to the ocean but not within a chevron. The samples contain only a small component of carbonate (S14: 3% $CaCO_3$ and S17: 9% $CaCO_3$). The samples contain no (S14) or very few (S17: 10 fossils/gm) marine microfossils. These samples are located above a small beach, a potential source for windblown sediment. Despite the nearshore location and a potential aeolian source area, the sediments from these two sites are poorly to moderately sorted.

elsevier_978-0-12-803386-9_B978-0-12-803386-9_00008-3

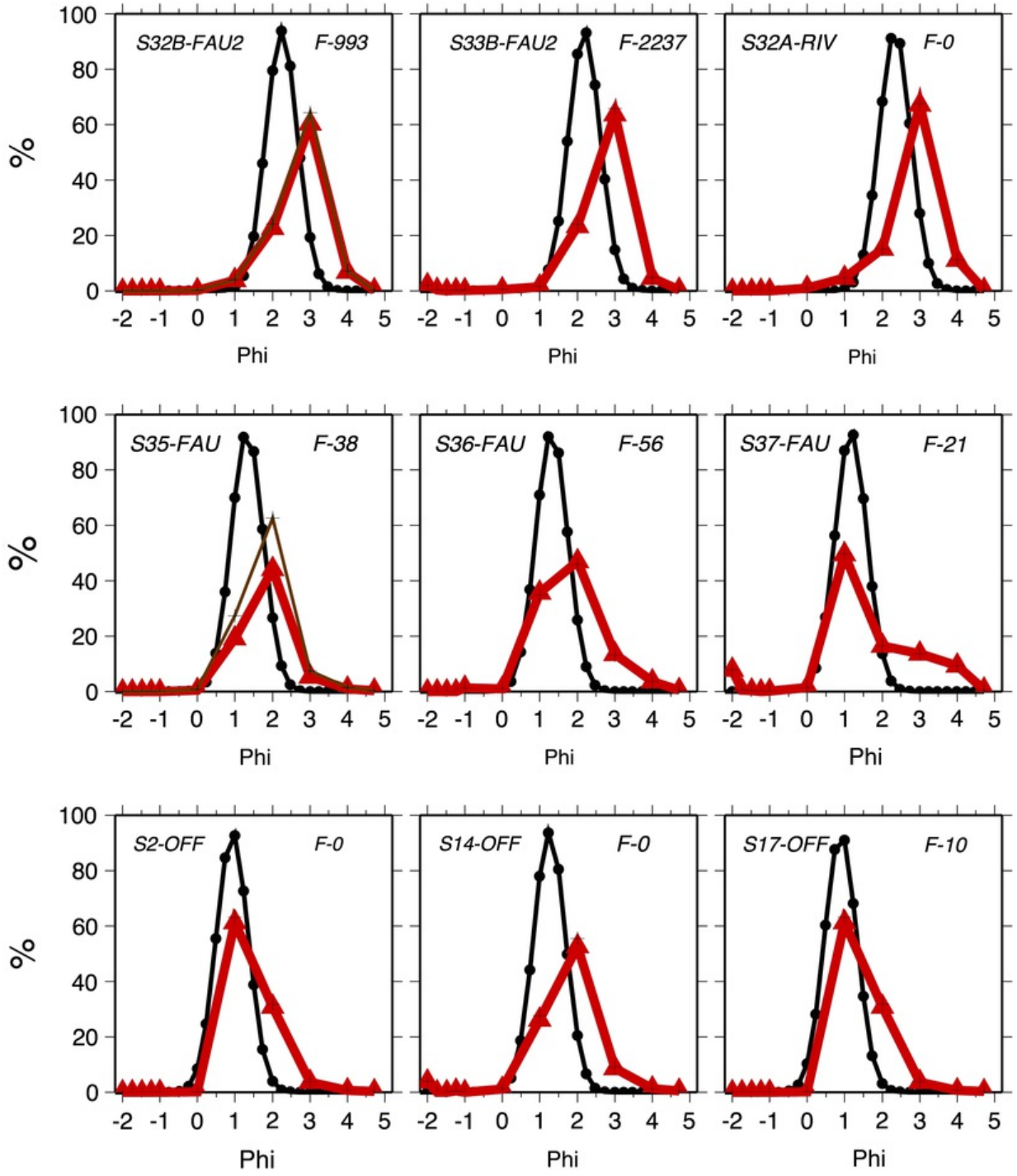

Figure 8.11 Grain size distribution of samples from the Faux Cap chevrons compared to samples from the Menarandra River (upper right) and from off chevron areas near Cap St. Marie and to the north (lower row of plots). *Black line* with *black dots*: Theoretical model of the grain size distribution of a well-sorted sand-a normal distribution with the same mean grain size as the sample. *Red line* with *triangles*: Grain size distribution uncorrected for material less than 38 μm in size. *Brown line* with *crosses*: Grain size distribution corrected to 100%, accounting for material washed through the 38 μm sieve, so not applicable to all samples. *F*, fossils per gram.

One site from the Faux Cap region located well away from the coast (S2, Fig. 8.11) and not on a chevron (Fig. 8.12: *green arrow*) has sand that contains no fossils and is moderately well sorted. It is one of the few samples with a mean grain size that lies within the mean grain size of well-sorted material. The other similar sample is S17, which is also off chevron and contains very few marine microfossils (Fig. 8.12). Samples S2 and S17 contain no material coarser than 0 ϕ (1000 μm), as might be expected of samples that are entirely (S2) or nearly entirely (S17) windblown material. There is some fine sand in S2 and S17 that keeps them from perfectly matching the size distribution of aeolian sand.

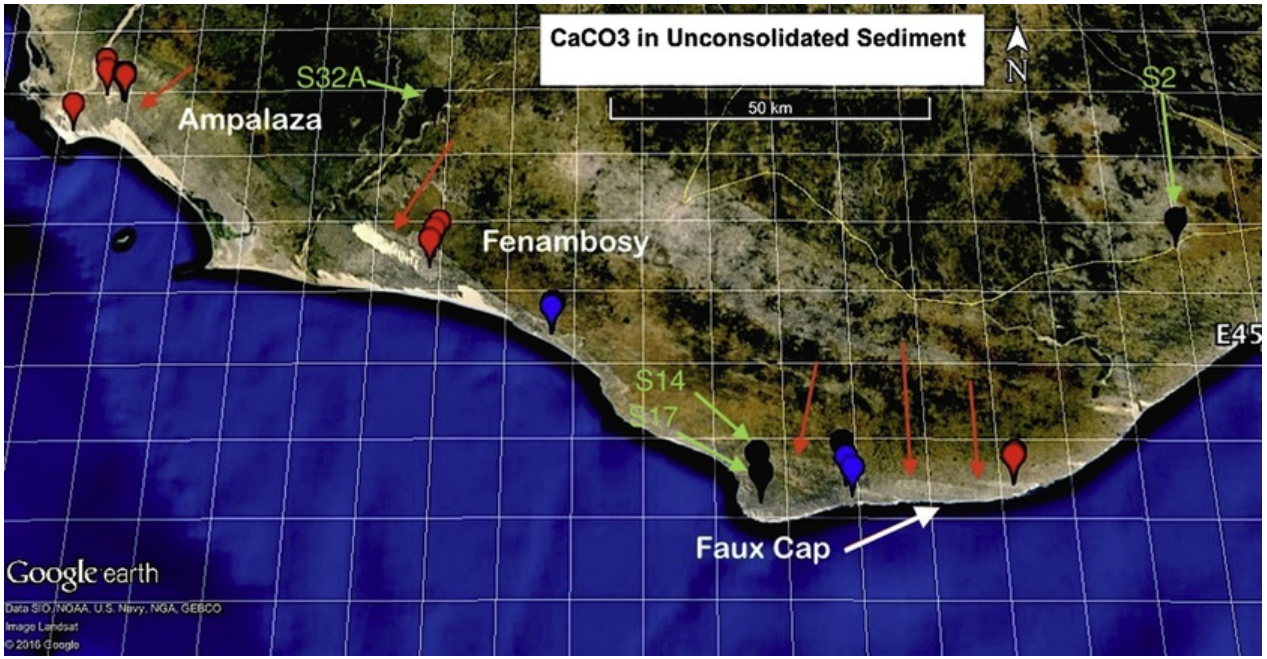

Figure 8.12 Summary of $CaCO_3$ content of chevrons and surrounding area. Image from Google Earth is contrast enhanced to show the chevrons. Image © 2016 DigitalGlobe. Image © 2016 CNES/Astrium. Colored symbols: Sampling locations color-coded by percentage of $CaCO_3$ in the sediment. Black: 0–20% $CaCO_3$, Blue: 20–40% $CaCO_3$: Red 40–60% $CaCO_3$. *Red arrows*: Landward edges of chevrons. *Green arrows*: Off chevron sampling sites S2, S14, S17, and S32A.

Within the chevrons, there is a direct relationship between calcium carbonate content and marine fossil content (Fig. 8.13). As fossil content increases, the average carbonate content increases. As the fossils become more ablated by the wind, they are more difficult to recognize and count. Thus, the fossil counts per gram represent a lower bound in some sediment.

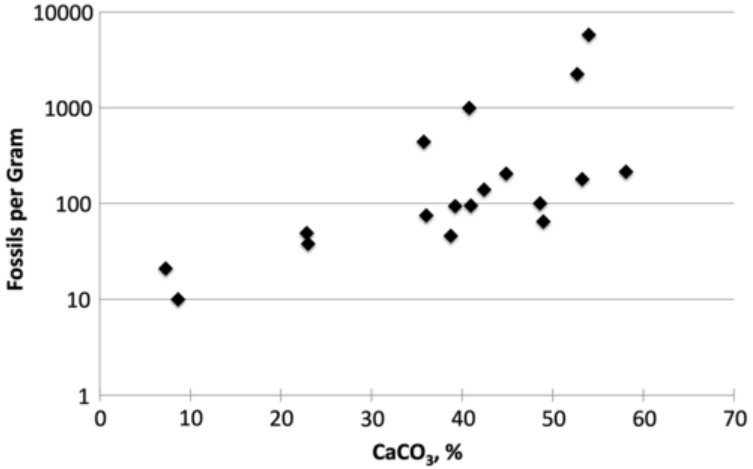

Figure 8.13 Bulk calcium carbonate content versus number of marine fossils per gram.

7 Discussion of Madagascar Chevrons

If the chevron sands were derived from the substrate, we would expect their fossil content and grain size distributions to be similar. If the chevron sands were transported inland from beaches by the wind, we would expect them to contain little to no calcium carbonate beyond a few km from the ocean, and no identifiable marine microfossils. We would also expect the associated mineral grains to be well rounded and well sorted (Sharp, 1966). This is not the case. Instead, sediments from locations that are tens of km along-strike in the chevrons contain marine microfossils (Figs. 8.5, 8.7, and 8.10) and significant $CaCO_3$ (summary in Fig. 8.12). The surrounding sedimentary grains are angular and typically moderately sorted to moderately well sorted (Figs. 8.6, 8.8, and 8.11).

The chevron sands are typically classified as either moderately well sorted or moderately sorted. This may be because the total weight of individual sieved samples is relatively small, about 20–30 g. The largest rocks are not abundant. There are often only one or two per sample. The presence of these larger rocks decreases estimates of the degree of sorting. Thus, the degree of sorting we estimate could be systematically too high. This putative sample size effect may explain why we did not find a large number of sites with poorly sorted sediment within the chevrons.

The presence of Mg-rich fills within the microfossils from the Ampalaza Chevron is complemented by microprobe analyses of individual fossil tests from this site (manuscript in preparation). Microprobe analyses show that MgO is present within the marine microfossil tests at the level of a few percent. This is significantly higher than the MgO content of modern marine foraminiferal tests, which is at most <1% (Nürnberg et al., 1996; Lear et al., 2000, 2002; Reichart et al., 2003). This is not enough MgO for the carbonate in the tests to be called dolomite, but it is enough to suggest that the tests experienced some diagenetic replacement. In dolomite-rich sediments, most of the dolomite is estimated to form within a few tens of m of the sediment–water interface (Baker and Burns, 1985). It is likely that the tests were buried in an environment where calcium carbonate was being replaced by dolomite, with burial long enough for the interiors of the tests to be filled with semilithified material, some with a high Mg content (Fig. 8.9).

8 Geochronology

We obtained AMS ^{14}C dates of the carbonate microfossils in the chevron sand in three widely separated locations (Figs. 8.14 and 8.15, Table 8.4). The ages of the carbonate range from 13,835 ± 40 to 11,415 ± 35 year BP. The ages of recent marine carbonates in the southwest tropical Indian Ocean vary from 418 ± 57 to 800 ± 59 year BP (Southon et al., 2002), much younger than the ages of the carbonate microfossils in the chevrons. These ages are not zero because older carbon is incorporated into modern marine calcium carbonate. The correction for this effect is called the marine carbonate reservoir correction.

elsevier_978-0-12-803386-9_B978-0-12-803386-9_00008-3

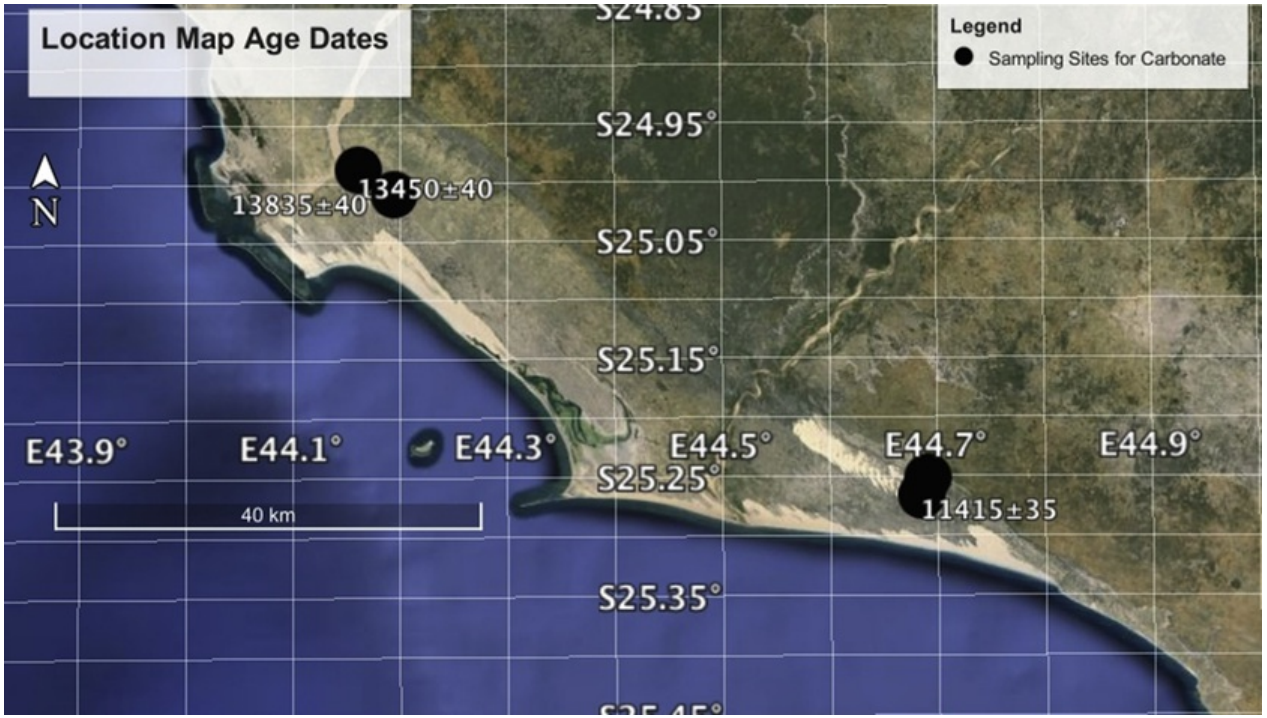

Figure 8.14 Location map of ^{14}C sampling sites (*black circles*). Annotations are uncorrected ages with errors. The Ampalaza Chevron on the left (west) has two similar ages. The Fenambosy Chevron on the right (east) has one final age determination and a second age in progress. Because the sand in the chevrons could have been derived from differing levels of erosion of preexisting sediments, all ages are maximum ages and do not preclude the same age of formation of both chevrons.

Figure 8.15 Top: White boulder and smaller rocks in farmer's field on top of 175 m high cliff. Middle: Foreground: Typical country rock. Background, middle right: Possible displaced boulders. Some appear white. Farmers seeking to maximize their crop yields may have cleared the smaller boulders from the fields. The red soil in the bank to the left contains no visible rocks and is an unlikely source for boulders of this size. Bottom: View of the ocean, 7 km from edge of cliff and from farmer's field shown above. Boulders here appear gray rather than white.

Table 8.4 Uncorrected Radiocarbon Ages of Marine Carbonate

CAMS#	Site Name	Fraction Modern	±	$\delta^{14}C$	±	^{14}C Age	±
172725	MAD 19	0.1874	0.0009	−812.6	0.9	13,450	40
172726	MAD 26	0.1787	0.0009	−821.3	0.9	13,835	40
172727	MAD 13	0.2414	0.0010	−758.6	1.0	11,415	35

9 Origin of the Madagascar Chevrons Investigated Here

The age of the chevrons is unknown but it must be geologically young. None of the chevrons are lithified and all the fossils appear as individual tests. Five sets of sedimentologic observations strongly suggest a water-laid, premodern

origin for the chevrons. The first is their unusual V-shaped appearance, and the low maximum slopes of the triangular sediment waves in the chevrons, on the order of 5–10 degrees. All of these sediment waves are covered by vegetation. Maximum slopes of water-laid sediment waves are typically <10 degrees, although they are occasionally as high as 20 degrees (Ashley, 1990). The second observation suggesting chevrons were deposited by a megatsunami is the absence of a trend in the degree of sorting along-strike of the chevrons. The sand in the Ampalaza and Fenambosy Chevrons is several m thick and would be expected to become well-sorted and well-rounded within 10–12 km of along-strike transport by the wind (Sharp, 1966). Instead the sediment in the chevrons varies in sorting but is typically either moderately well sorted or moderately sorted. The third observation is the difference in maximum slope and shape of the sand waves between the vegetated and unvegetated areas of the chevrons. The sand waves in the white areas form long dunes oriented at right angles to the wind direction. The maximum slopes of the white sand waves on their dip-slopes are 30 degrees, the expected slope for dunes of windblown origin. Therefore, the sand waves in the white, unvegetated areas of the chevrons have experienced a different recent history from the sand waves in the vegetated areas of the chevrons. The fourth is the form, composition, and excellent preservation of the microfossils in the chevrons. The microfossils are abundant and are often filled with Mg-rich material. Their abundance does not decrease along-strike of the chevrons. If the chevrons were entirely of windblown origin, we infer that well-preserved microfossils would be absent beyond 10–12 km along-strike. Instead we see abundant, well-preserved microfossils at distances of tens of km along-strike, including at the most distal end of the Ampalaza Chevron. The sandy substrate of the chevrons contains little carbonate and no fossils (Figs. 8.5, 8.7, and 8.10). There is no or less than 10% $CaCO_3$ and no or sparse marine fossils in sands from the areas surrounding the chevrons (Fig. 8.12). The fifth important observation is that the Ampalaza Chevron is buried on its eastern end by floodplain sediments from the Menarandra River. If the chevrons were modern features that were actively forming through aeolian transport of beach and fluvial sand, we would expect to see well-preserved V-shaped chevrons immediately west of the bank of the Menarandra River. There are possibly a few relict chevrons being farmed in this area (Fig. 8.7: top) but they appear to be partially reworked by the wind.

These sedimentologic observations are consistent with a megatsunami origin for these chevrons; geochronological data help to pinpoint the timing of such an event. Because we infer that carbonate was most likely eroded from a preexisting, fossil-bearing sediment, the ages of the carbonate particles in the sediment are roughly the same as the age of the depositional event and older. That is, the ^{14}C ages are maximum ages for the megatsunami. Considering that these are maximum ages, the range of ages is small. Further, these ages constitute additional evidence that the chevrons are not modern aeolian deposits derived from local beaches. If the carbonate microfossils in the chevrons were blown in from nearby beaches, the ages of the carbonate in the chevrons would be close to or within the range of the reservoir correction for the Indian Ocean. While it is conceivable that nondegraded or lightly degraded fossil shell is present in the littoral margin of southern Madagascar, and could be incorporated into aeolian deposits, and while our radiocarbon sample size is quite small, our overall project data suggest that the chevron deposits are water-laid, and date prior to the late Holocene or modern era.

The ^{14}C age results also appear to preclude another hypothesis: that the individual marine carbonate tests are being eroded from poorly lithified carbonate-rich rocks in the basement. If the carbonate tests were derived from the basement, they would be radiocarbon dead, giving inconclusive ages of >45,000 years.

10 Other Modern Tsunami Deposits: Mixtures of Carbonate-Rich Sand and Large Rocks

Studies of tsunami deposits in modern environments show that mixtures of calcium carbonate-rich sand and large rocks, often of megaboulder size, are common. There are numerous well-documented examples of boulders transported inland by tsunamis (Bryant et al., 1992; Scheffers and Kelletat, 2003; Scicchitano et al., 2007; Paris et al., 2010; Bryant, 2014). Where other sediments are present, the boulders are often in stratigraphic contact with carbonate- and/or silicate-rich sand.

Large boulders and sand sheets deposited from a megatsunami have been documented in the Cape Verde islands (Ramalho et al., 2015). The sand layers contain dispersed rounded and angular clasts. The maximum run-up heights are in excess of 270 m. The megatsunami was produced from a caldera collapse of Fogo volcano about 73,000 years ago.

In Madagascar, there are white boulders within the sands at the top of the 175-m high cliff within the Fenambosy Chevron. Because they are too large for subsistence farmers to move without mechanical assistance, large boulders lie within a field that is being actively farmed (Fig. 8.15; top). Other rocks appear in piles within depressions in the country rock. The whiter rocks lack the dark coating of the basement rock (Fig. 8.15; middle). The white boulders might represent more recent deposits with insufficient time to develop a dark weathering rind. These boulders need to be investigated in more detail, to determine if they were torn from the edge of the cliff or if they were transported over a longer distance (Fig. 8.15; bottom).

11 Suggestions for Further Work

Many workers have documented the presence of foraminifera within tsunami deposits (Mamo et al., 2009; Sugawara et al., 2009; Pilarczyk and Reinhardt, 2012). We know of no other cases where the foraminifera within tsunami deposits are filled in and partially dolomitized; however, most researchers do not make thin sections of foraminifera or examine them with a scanning electron microscope. In the future, it would be helpful to know if the dolomitization of marine microfossils is nonuniform within tsunamigenic sequences. In areas where dolomitization of offshore sequences is favored, the maximum amount of dolomitization might correlate well with the degree of erosion of offshore sediments by the tsunami, a likely marker for tsunami size.

The high carbonate contents of the Madagascar chevrons suggest that multispectral remote sensing data should be able to evaluate the carbonate content of other V-shaped dune complexes. In tropical regions, coastal chevron dunes with high carbonate contents should be identified and studied to determine their age and origin.

Once modern shoreline tsunami deposits are more fully documented, it will be possible to identify more of their counterparts within Precambrian and Phanerozoic sediments. Although Precambrian carbonates were not precipitated as shells, their precipitation was modulated by a low rate of deposition of clastic material. In areas with a high rate of clastic deposition, carbonate precipitation is overwhelmed and the sediment subsequently becomes a shale or sandstone. Thus, the admixture of large amounts of fine-grained carbonate or dolomite with significant amounts of sand, gravel, or boulders suggests some special circumstances. If the sedimentary structures are also appropriate, such mixed carbonate-coarse clastic sequences could represent ancient megatsunami deposits.

The Madagascar chevrons show that the stratigraphic expression of ancient tsunami deposits on shorelines is likely to be complicated. The water-laid sand waves of low amplitude have been preserved by vegetation in some parts of the chevrons but in other areas the sand is being actively eroded and reworked by the wind. Because there was little to no vegetation during Precambrian time (Long, 2011; Eriksson et al., 2013; Mazumder and Van Kranendonk, 2013), this mixed stratigraphic expression of tsunami deposits could be present in Precambrian sequences. In addition, the high carbonate content of the Madagascar chevrons, typically 30–50%, suggests that abundant carbonate sand mixed with sand, gravel, or boulders that are not carbonate and/or of differing carbonate/dolomite content could be a marker for ancient tsunami deposits (Lowe and Byerly, 1988; Hassler et al., 2000; Hassler and Simonson, 2001; Glikson, 2004; Glass and Simonson, 2012; Lowe et al., 2014). We find that the average bulk carbonate content in the Madagascar sediments is directly related to the fossil content per unit weight (Fig. 8.14). This implies that similar mixed carbonate-sand-gravel-boulder sequences in ancient sediments should be assessed for current structures and sediment waves, characteristic of aqueous deposition.

Appendix 8.1: Weight Percentage Data of Different Grain Sizes Used to Calculate Grain Size Parameters in Table 8.2

Station Number	>4000	>3360	>2800	>2360	>2000	>1000	>500	>250	>125	>63	>38	Sum
S2	0.0	0.0	0.0	0.0	0.0	0.2	61.3	30.9	3.7	0.7	0.4	97.2
S4	0.0	0.2	0.0	0.4	0.8	2.0	5.7	28.8	38.0	11.3	2.3	89.4
S5	1.0	0.2	0.0	0.1	0.0	0.0	2.1	70.5	23.0	1.0	0.3	98.1
S9	0.0	0.1	0.0	0.0	0.0	0.2	31.6	14.6	38.8	11.0	0.4	96.7
S12	0.5	0.6	0.7	0.2	0.1	0.5	0.8	8.2	70.5	13.2	0.4	95.6
S13	0.2	0.2	0.0	0.0	0.0	0.2	14.0	23.6	37.1	4.4	0.3	80.1
S14	3.8	0.0	0.0	0.5	0.0	1.2	26.2	52.7	8.7	1.3	0.5	94.9
S17	0.0	0.1	0.0	0.1	0.0	2.7	57.3	34.0	3.7	0.3	0.1	98.4
S19	0.0	0.0	0.0	0.0	0.0	0.0	0.0	4.8	73.3	19.9	0.1	98.1
S20	0.0	0.0	0.0	0.0	0.0	0.0	0.5	24.7	62.4	10.6	0.1	98.3
S22	0.0	0.0	0.0	0.0	0.0	0.0	0.1	1.4	54.8	41.4	0.4	98.0
S25	0.0	0.0	0.0	0.0	0.0	0.2	3.3	26.3	58.9	8.3	0.4	97.5
S26	0.0	0.0	0.0	0.0	0.0	0.1	21.8	27.0	44.9	3.5	0.1	97.4
S27	0.0	0.0	0.0	0.0	0.0	0.1	8.9	25.3	52.2	9.6	0.5	96.5
S28	0.0	0.0	0.0	0.0	0.0	0.0	14.5	42.1	34.5	2.9	0.7	94.7
S30	0.3	0.0	0.1	0.1	0.0	0.6	8.7	39.5	47.0	2.2	0.1	98.7
S32A	0.0	0.0	0.0	0.0	0.0	1.0	4.7	15.1	67.1	11.1	0.3	99.3
S32B	0.0	0.0	0.0	0.0	0.0	0.2	3.8	22.7	60.4	6.8	0.1	94.0
S33	2.0	0.3	0.1	0.1	0.2	0.6	1.5	23.4	63.6	4.7	0.3	96.6

S35	0.0	0.0	0.0	0.0	0.0	0.5	19.2	44.1	5.3	1.0	0.3	70.5
S36	0.0	0.0	0.0	0.0	1.3	0.9	34.5	45.4	13.0	3.6	0.5	99.2
S37	7.8	0.5	0.3	0.0	0.1	1.5	49.6	16.5	13.6	9.3	0.6	99.8

Sizes of grains are in μm.

References

Abbott D.H., Bryant E.F., Gusiakov V., Masse W. and Breger D., Impacts, mega-tsunami, and other extraordinary claims: COMMENT, *GSA Today* **18** (6), 2008, e12.

Abbott D.H., Masse W.B., Burckle L.H., Breger D. and Gerard-Little P., Burckle abyssal impact crater: did this impact produce a global deluge?, In: Papmarinopoulous S.P., (Ed), *The Atlantis Hypothesis: Searching for a Lost Land,* 2007, Heliotopos Publications; Greece, 179–190.

Allen J.R.L., Principles of Physical Sedimentology, 1985, Chapman and Hall.

Ashley G.M., Classification of large-scale subaqueous bedforms: a new look at an old problem-SEPM bedforms and bedding structures, *Journal of Sedimentary Petrology* **60** (1), 1990, 160–172.

Baker P.A. and Burns S.J., Occurrence and formation of dolomite in organic-rich continental margin sediments, *AAPG Bulletin* **69** (11), 1985, 1917–1930.

Blott S.J. and Pye K., GRADISTAT: a grain size distribution and statistics package for the analysis of unconsolidated sediments, *Earth Surface Processes and Landforms* **26**, 2001, 1237–1248.

Bourgeois J. and Weiss R., “Chevrons” are not mega-tsunami deposits—A sedimentologic assessment, *Geology* **37** (5), 2009, 403–406.

Bryant E., Tsunami: The Underrated Hazard, 2014, Springer.

Bryant E.A. and Nott J., Geological indicators of large tsunami in Australia, *Natural Hazards* **24** (3), 2001, 231–249.

Bryant E.A., Young R.W. and Price D.M., Evidence of tsunami sedimentation on the southeastern coast of Australia, *The Journal of Geology* **1**, 1992, 753–765.

Camoin G.F., Montaggioni L.F. and Braithwaite C.J.R., Late glacial to post glacial sea levels in the Western Indian Ocean, *Marine Geology* **206** (1), 2004, 119–146.

Cox R., Zentner D.B., Kirchner B.J. and Cook M.S., Boulder ridges on the Aran Islands (Ireland): recent movements caused by storm waves, not tsunamis, *The Journal of Geology* **120** (3), 2012, 249–272.

De Villiers S., Foraminiferal shell-weight evidence for sedimentary calcite dissolution above the lysocline, *Deep Sea Research Part I: Oceanographic Research Papers* **52** (5), 2005, 671–680.

Erdmann W., Kelletat D., Scheffers A.M. and Haslett S., Origin and Formation of Coastal Boulder Deposits at Galway Bay and the Aran Islands, 2015, Heidelberg Springer Briefs in Geography; Western Ireland.

Eriksson P.G., Banerjee S., Catuneanu O., Corcoran P.L., Eriksson K.A., Hiatt E.E., Laflamme M., Lenhardt N., Long D.G.F., Miall A.D., Mints M.V., Pufahl P.K., Sarkar S., Simpson E.L. and Williams G.E., Secular changes in sedimentation systems and sequence stratigraphy, *Gondwana Research* **24**, 2013, 468–489.

Glass B.P. and Simonson B.M., Distal impact ejecta layers: Spherules and more, *Elements* **8**, 2012, 43–48.

Glikson A.Y., Early Precambrian asteroid impact-triggered tsunami: excavated seabed, debris flows, exotic boulders, and turbulence features associated with 3.47–2.47 Ga-old asteroid impact fallout units, Pilbara craton, western Australia, *Astrobiology* **4** (1), 2004, 19–50.

Gusiakov V., Abbott D.H., Bryant E.A., Masse W.B. and Breger D., Mega tsunami of the world oceans: chevron dune formation, micro-ejecta, and rapid climate change as the evidence of recent oceanic bolide impacts, In: Beer T., (Ed), *Geophysical Hazards, Minimizing Risk, Maximizing Awareness Netherlands,* 2010, Springer, 197–227.

Hassler S.W., Robey H.F. and Simonson B.M., Bedforms produced by impact-generated tsunami, ~2.6 Ga Hamersley basin, Western Australia, *Sedimentary Geology* **135** (1), 2000.

Hassler S.W. and Simonson B.M., The sedimentary record of extraterrestrial impacts in deep-shelf environments: evidence from the early Precambrian, *The Journal of Geology* **109**, 2001, 1–19.

Hearty P.J., Neumann A.C. and Kaufman D.S., Chevron ridges and runup deposits in the Bahamas from storms late in oxygen-isotope substage 5e, *Quaternary Research* **50** (3), 1998, 309–322.

elsevier_978-0-12-803386-9_B978-0-12-803386-9_00008-3

Kindler P. and Strasser A., Palaeoclimatic significance of co-occurring wind-and water-induced sedimentary structures in the last-interglacial coastal deposits from Bermuda and the Bahamas, *Sedimentary Geology* **131** (1), 2000, 1–7.

Krumbein W.C. and Pettijohn F.J., Manual of Sedimentary Petrography, 1938, Appleton-Century-Crofts; New York.

Lear C.H., Elderfield H. and Wilson P.A., Cenozoic deep-sea temperatures and global ice volumes from Mg/Ca in benthic foraminiferal calcite, *Science* **287** (5451), 2000, 269–272.

Lear C.H., Rosenthal Y. and Slowey N., Benthic foraminiferal Mg/Ca-paleothermometry: a revised core-top calibration, *Geochimica et Cosmochimca Acta* **66** (19), 2002, 3375–3387.

Long D.G.F., Architecture and depositional style of fluvial systems before land plants: a comparison of Precambrian, early Paleozoic and modern river deposits, In: Davidson S.K., Leleu S. and North C.P., (Eds.), *From River to Rock Record: The Preservation of Fluvial Sediments and Their Subsequent Interpretation* **vol. 97**, 2011, SEPM Special Publication, 37–61.

Lowe D.R. and Byerly G.R., Identification and effects of large, early Archean, terrestrial meteorite impacts: a geological perspective on late accretion, In: *Proceedings Lunar and Planetary Science Conference* **vol. 19**, 1988, Lunar and Planetary Institute; Houston, TX, 693.

Lowe D.R., Byerly G.R. and Kyte F.T., Recently discovered 3.42–3.23 Ga impact layers, Barberton Belt, South Africa: 3.8 Ga detrital zircons, Archean impact history, and tectonic implications, *Geology* **42** (9), 2014, 747–750.

Mamo B., Strotz L. and Dominey-Howes D., Tsunami sediments and their foraminiferal assemblages, *Earth-Science Reviews* **96** (4), 2009, 263–278.

Maxwell T.A. and Haynes C.V., Large-scale, low-amplitude bedforms (chevrons) in the selima sand sheet, Egypt, *Science* **243** (4895), 1989, 1179–1182.

Mazumder R. and Van Kranendonk M.J., Paleoproterozoic terrestrial sedimentation in the Beasley river quartzite, lower Wyloo Group, western Australia, *Precambrian Research* **231**, 2013, 98–105.

Nürnberg D., Bijma J. and Hemleben C., Assessing the reliability of magnesium in foraminiferal calcite as a proxy for water mass temperatures, *Geochimica et Cosmochimica Acta* **60** (5), 1996, 803–814.

Oehler J.F., Labazuy P. and Lénat J.F., Recurrence of major flank landslides during the last 2-Ma-history of Reunion Island, *Bulletin of Volcanology* **66** (7), 2004, 585–598.

Paris R., Fournier J., Poizot E., Etienne S., Morin J., Lavigne F. and Wassmer P., Boulder and fine sediment transport and deposition by the 2004 tsunami in Lhok Nga (western Banda Aceh, Sumatra, Indonesia): a coupled offshore–onshore model, *Marine Geology* **268**, 2010, 43–54.

Pilarczyk J.E. and Reinhardt E.G., Testing foraminiferal taphonomy as a tsunami indicator in a shallow arid system lagoon: Sur, Sultanate of Oman, *Marine Geology* **295**, 2012, 128–136.

Pinter N. and Ishman S.E., Impacts, mega-tsunami, and other extraordinary claims, *GSA Today* **18** (1), 2008, 37–38.

Ramalho R.S., Winckler G., Madeira J., Helffrich G.R., Hipólito A., Quartau R., Adena K. and Schaefer J.M., Hazard potential of volcanic flank collapses raised by new megatsunami evidence, *Science Advances* **1** (9), 2015.

Reichart G.J., Jorissen F., Anschutz P. and Mason P.R., Single foraminiferal test chemistry records the marine environment, *Geology* **31** (4), 2003, 355–358.

Scheffers A. and Kelletat D., Sedimentologic and geomorphologic tsunami imprints worldwide—A review, *Earth-Science Reviews* **63**, 2003, 83–92.

Scheffers A., Kelletat D., Scheffers S.R., Abbott D.H. and Bryant E.A., Chevrons–enigmatic sedimentary coastal features, *Zeitschrift für Geomorphologie* **52** (3), 2008, 375–402.

Scicchitano G., Monaco C. and Tortorici L., Large boulder deposits by tsunami waves along the Ionian coast of south-eastern Sicily (Italy), *Marine Geology* **238**, 2007, 75–91.

Sharp R.P., Kelso dunes, Mojave desert, California, *Geological Society of America Bulletin* **77**, 1966, 1045–1074.

Skoček V. and Saadallah A.A., Grain-size distribution, carbonate content and heavy minerals in eolian sands, southern desert, Iraq, *Sedimentary Geology* **8** (1), 1972, 29–46.

Southon J., Kashgarian M., Fontugne M., Metivier B. and Yim W.W., Marine reservoir corrections for the Indian Ocean and Southeast Asia, *Radiocarbon* **44** (1), 2002, 167–180.

Sugawara D., Minoura K., Nemoto N., Tsukawaki S., Goto K. and Imamura F., Foraminiferal evidence of submarine sediment transport and deposition by backwash during the 2004 Indian Ocean tsunami, *Island Arc* **18** (3), 2009, 513–525.

Visher G.S., Grain size distributions and depositional processes, *Journal of Sedimentary Research* **39** (3), 1969, 1074–1106.

Woodroffe S.A. and Horton B.P., Holocene sea-level changes in the Indo-Pacific, *Journal of Asian Earth Sciences* **25** (1), 2005, 29–43.

Abstract

Madagascar chevrons are V-shaped, coastal dunes of disputed origin. Three distinct chevron complexes were sampled in this chapter: Fenambosy, Ampalaza, and Faux Cap. Chevrons contain abundant carbonate marine microfossils, some partially dolomitized, deposited over along-strike distances of 12 to >40 km. Marine microfossils in the dunes resemble filled-in marine foraminifers, differing from the hollow tests that dominate local beach deposits, and therefore arguing against modern beach deposits being the source of the chevrons' carbonate sands. Chevron dunes sampled in this study are typically not well sorted, with sediment surfaces that slope ≤10 degree. Both observations are inconsistent with an aeolian origin for the deposits. AMS ^{14}C dating of three carbonate-rich sands yields ages between 13,835 ± 40 and 11,415 ± 35 years before present (year BP), significantly older than modern marine carbonate sediments aged 800 to 418 year BP (i.e., the marine reservoir correction). Assuming that the age range stipulated for carbonate sand represents the maximum plausible age of deposition of the chevrons also argues against a modern aeolian origin. Taken together, characteristics of the chevrons instead support the inference that they are megatsunami deposits possibly related to a Holocene landslide or bolide impact.

Queries and Answers

Query: As per style, the author names are abbreviated. Kindly check.
Answer: The names are correct.

Query: Please check the edit made in affiliation of author “V. Gusiakov”.
Answer: I changed it and added Tsunami Laboratory

Query: Please provide city name.
Answer: Antananarivo

Query: Please check the edit made in affiliation of author “R. Mazumder”.
Answer: The affliation is correct.

Query: Please provide Keyword for this chapter.
Answer: tsunami, chevron, dune, microfossil

Query: Please check if the version of image used is correct.
Answer: Yes the image in the top part of figure 8.4 is correct

Query: Please check if the version of image used is correct.
Answer: Yes figure 8,6 is correct